Damage evolution in fuselage stiffened composite panels under asymmetrical bending loading conditions

Cite as: AIP Conference Proceedings **2309**, 020033 (2020); https://doi.org/10.1063/5.0033945
Published Online: 30 November 2020

Valerio Acanfora, Andrea Sellitto, Aniello Riccio, and Francesco Di Caprio

Damage Evolution in Fuselage Stiffened Composite Panels Under Asymmetrical Bending Loading Conditions

Valerio Acanfora[1, a)], Andrea Sellitto[1, b)], Aniello Riccio[1, c)], and Francesco Di Caprio[2 ,d)]

[1]*University of Campania "Luigi Vanvitelli", Department of Engineering, via Roma 29, 81031, Aversa (CE), Italy.*
[2]*Italian Aerospace Research Centre (CIRA), via Maiorise snc, 81043, Capua (CE), Italy.*

[a)]Corresponding author: valerio.acanfora@unicampania.it
[b)]andrea.sellitto@unicampania.it
[c)]aniello.riccio@unicampania.it
[d)]f.dicaprio@cira.it

Abstract. In this paper, the damage mechanisms of reinforced composite panels subjected to symmetrical and asymmetrical flexural loading conditions have been investigated. The composite components are representative of a regional aircraft fuselage. Three-point bending tests numerical simulations have been used to assess the influence of the different test parameters on the damage behavior of the investigated component. Then, the most representative configuration has been selected for the experimental bending test. the outputs from the numerical simulations, in terms of stiffness and damage onset and propagation, has been employed, in combination with the experimental data, to accurately describe the damage mechanisms associated to the asymmetric application of the load.

INTRODUCTION

The use of fiber-reinforced composites is constantly growing in aerospace applications, thanks to their lightweight characteristic combined with highly resistant capability. However, due to the low mechanical capabilities of the matrix, they are characterized by a brittle behavior in the direction normal the lamination plane, which can result in the onset of delaminations during service conditions. Hence, it becomes mandatory to deeply investigate the damage mechanisms of composite materials during their life cycle. Actually, aerospace structures are subjected to different critical loading conditions. Among these, asymmetrical loading conditions, arising during asymmetrical maneuvers and in general due to asymmetrical aerodynamic conditions, can have severe consequences on structural components of the fuselage, in terms of amplification the damage mechanisms [1]. Moreover, asymmetric loads can be generally dangerous for all types of structures, and even the simplest ones. In particular, in [2] a fatal accident at a warehouseman, due to asymmetrically loaded civil structures, was investigated, highlighting that the asymmetric loads reduce the critical instability load respect to a symmetric load. Even in structural elements such as sandwich panels, asymmetrical loads change the evolution of the damage mechanisms. In fact, the work [3] shows that in case of asymmetrically loaded systems, the flexural rigidity increases significantly compared to symmetrical loaded systems causing sudden collapses. At the moment, however, there are not many works that investigate the initial and propagation phase of the damage mechanisms on structures loaded with asymmetrical loads. Among them, there are some works [4-6] that presents excellent numerical methods for damage assessment in circular cylindrical shell subjected to asymmetric loads. It is therefore necessary investigate the damage processes caused by asymmetric loading applications on composite structures. Moreover, as flexural loading represents a very critical loading conditions for structures, it is interesting to explore the damage mechanisms of complex composite structures, composed by skin and stringer, subjected to asymmetrical flexural load. Indeed, during flexural loads, the debonding phenomenon between skin and stringer is frequent to occur [7,8]. Also debonding, due to the fact that it

Fracture and Damage Mechanics
AIP Conf. Proc. 2309, 020033-1–020033-10; https://doi.org/10.1063/5.0033945
Published by AIP Publishing. 978-0-7354-4045-6/$30.00

is a damage mechanism usually not visible to the human eye, can lead to sudden collapses of the structure [7-12]. Therefore, it is prudent and interesting to explore the development of intra-laminar and inter-laminar damage mechanisms [13-15], including debonding, during the application of asymmetric bending loads.

Because of these considerations, the present paper introduces a numerical-experimental investigation on the mechanical behavior of a CFRP stiffened panel subjected to asymmetrical loading conditions. Indeed, to assess the effect, in terms of onset and evolution of the inter-laminar and intra-laminar damages, of the asymmetrical boundary conditions, a comparison between symmetrical and asymmetrical configurations has been performed. Several stiffened panel configurations, obtained by modifying the geometrical dimensions of the panel and the orientation of the roll in the 3-points bending kit, has been numerically analyzed. Then, the most representative configuration has been selected for the experimental bending test. Resulting experimental data, in terms of stiffness variation with the load application and skin-stringer debonding area, have been assumed to measure the mechanical performances of the stiffened panel. Images from a non-destructive test with a Phased Array Ultrasound techniques have been adopted together with the outputs from the numerical simulations, in terms of intra-laminar and inter-laminar damages onset and evolution, to accurately describe the damage mechanisms associated to the asymmetrical application of the load leading to the premature collapse of the stiffened panel. In the following sections, the considered stiffened panels configurations are introduced. Then, the numerical results achieved from the symmetrical and the asymmetrical configurations are reported and, finally, experimental data on the selected asymmetrical configuration are assessed and correlated to numerical results to describe the damage mechanisms onset and evolution.

DESCRIPTION OF THE ANALYSED CONFIGURATIONS

Figure 1-a shows the Carbon Fiber Reinforced Polymer (CFRP) stiffened omega stringer co-cured panel configuration, studied in the frame of the work. This panel is a typical slice of a regional aircraft fuselage.

The commercial FEM software Abaqus standard has been chosen as environment for the FE models definition and for the numerical simulations of the three-point bending test used to evaluate the panel flexural behavior. Figure 1-b introduces the geometric characteristics of the panel and rollers adopted for the three-point bending tests.

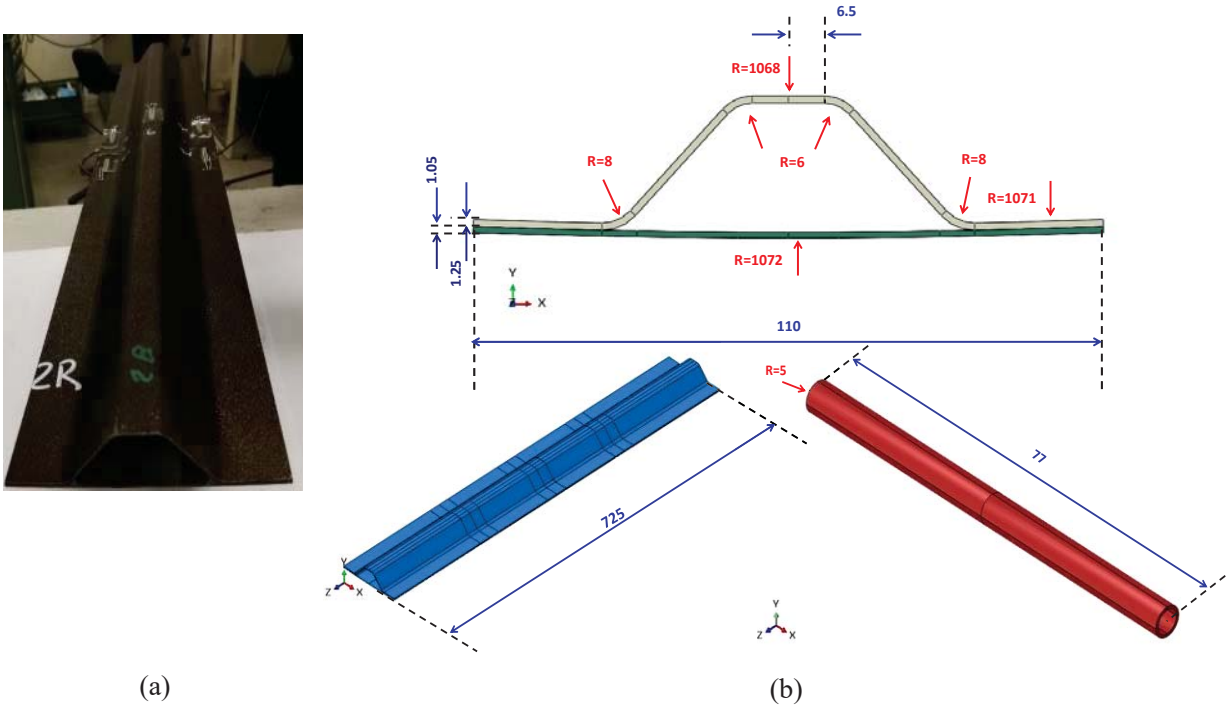

FIGURE 1. (a) Investigated CFRP reinforced panel; (b) geometric characteristics.

Three different FE numerical models have been defined to assess the symmetrical and asymmetrical bending conditions. These FE models adopted for the simulations are summarized in Figure 2, where the boundary conditions are detailed. Actually, three models have been introduced:

- A Symmetrical model, (identified as *Numerical_Symmetrical_model – NS*) which has been adopted to simulate the flexural behavior during a numerical symmetrical three-point bending test for comparison purposes with the asymmetrical tests.
- A first Asymmetrical model, (identified as *Numerical_Asymmetrical_model – NA*), which is characterized by an asymmetrical condition in the panel geometries obtained cutting, if compared to the symmetrical panel, one of the two caps by 50%.
- A second Asymmetrical model, (identified as *Numerical_Asymmetrical_RollerRotation_model* – NARR), which is characterized by the same asymmetrical geometrical condition characterizing the previous model combined with an asymmetry in the loading application introduced by rotating the lower roller (the one that imposes the displacement on the skin) around the x axis (in Figure 1-b) by 0.15 rad. In such a way, the displacement is not applied along the axis of symmetry of the panel, but instead in a stiffer area, identified by the presence of both skin and stringer.

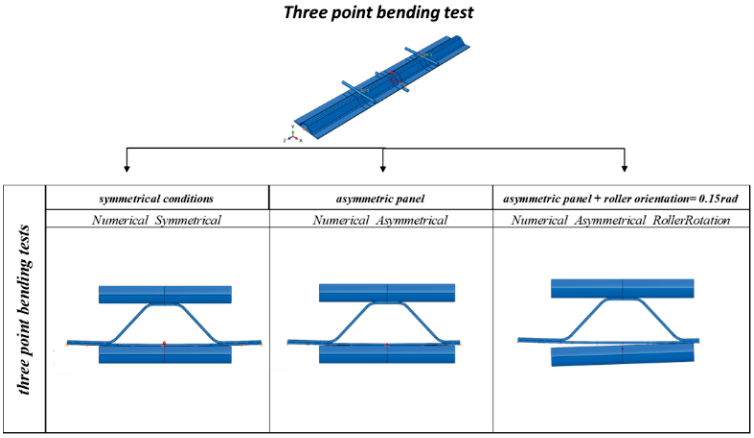

FIGURE 2. Definition of the numerical models.

The comparisons between the numerical output of the investigated configurations, have been performed in terms of:

- Load/applied displacement curves;
- Intra-laminar damages onset and propagation;
- Inter-laminar damages onset and propagation.

A preliminary mesh convergence analysis has been carried out in order to determine the discretization able to guarantee the optimal compromise between the computational cost of the analysis and the accuracy of the numerical results. Therefore, three different mesh sets, identified as *1s*, *2s*, and *3s* have been considered. These mesh sets are characterized by differences in the number of elements in the regions with increasing curvature (zones 1, 2, 3, and 4 in Figure 3-a), while the same discretization has been applied in the rest of the model. Abaqus SC8R 8-node continuum shell elements with a reduced integration scheme have been used to discretize the finite element models. Actually, contact elements, with a size of 1.5×2.5 mm^2, have been used between the roller and the panel, while elements with a size of 3×2.5 mm^2 have been used in the remaining part of the models except for zones 1, 2, 3, and 4. For both the skin and stringer meshes, only one element along the thickness has been adopted. The mesh sets, considered in the frame of the preliminary sensitivity analysis, are shown in Figure 3.

For each mesh set, a three-point bending test has been numerically simulated, by imposing a 3 mm displacement to the top roller and by considering the bottom rollers clamped. Table 1 reports the maximum values of the reaction force in the applied displacement direction and the computational cost of each numerical analysis.

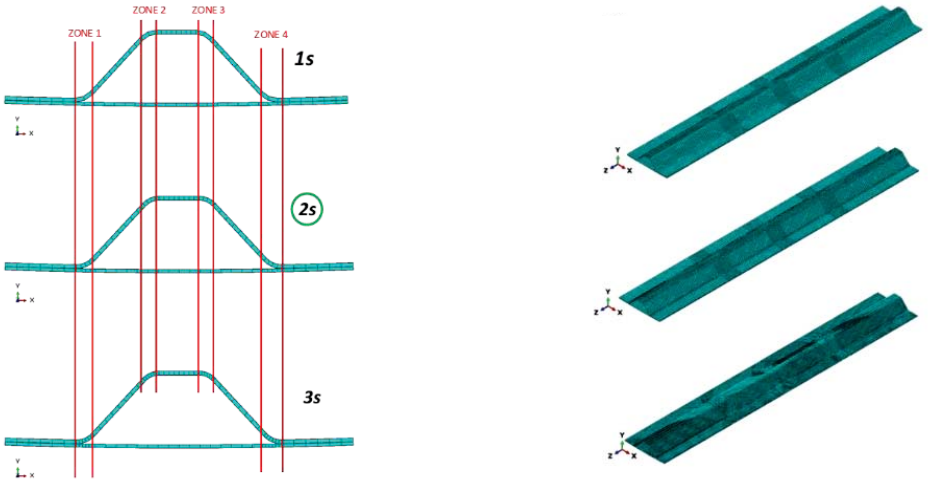

(a) (b)

FIGURE 3. Mesh sets. (a) X-Y plane; (b) 3D.

TABLE 1. convergence analysis output

Mesh set	N° elements in zone 1-4	RF max [kN]	Computational time [min]
1s	2	2.1	25
2s	4	2.45	53
3s	6	2.54	269

Figure 4-a shows the load-displacement trends for the analyzed mesh sets, while Figure 4-b shows the reaction force as a function of the analysis computational cost. According to the results shown in Table 1 and Figure 4, the mesh set *2s* has been identified as the one providing the best compromise between accuracy and computation cost. Indeed, a variation of about 4 % in the maximum reaction force with respect to the finer mesh set *3s* has been observed, with a significant saving in terms of computational time (about 5 times lower than the one needed for the *3s* mesh set analysis).

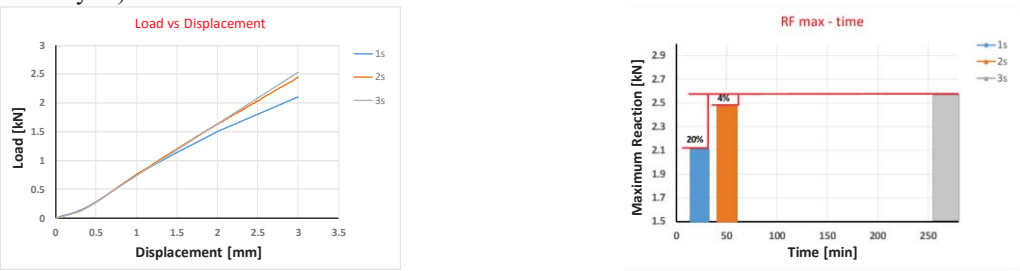

(a) (b)

FIGURE 4. Graphical comparison of mesh types: (a) reaction force vs imposed displacement; (b) maximum reaction force vs computational time.

NUMERICAL RESULTS

In this section, the numerical results obtained for the different configurations are presented, pointing out the influence of the asymmetrical geometrical and boundary conditions on the flexural stiffness and on the inter-laminar and intra-laminar damages onset and evolution. Comparing *Numerical_Symmetrical* and *Numerical_Asymmetrical* analysis, the impact of the geometrical asymmetry can be appraised. Indeed, the *Numerical_Asymmetrical* configuration has a cap 50% shorter respect to the *Numerical_Symmetrical* reference configuration. The different behavior of the two models is highlighted in Figure 5, where the load vs. imposed displacement curves are shown.

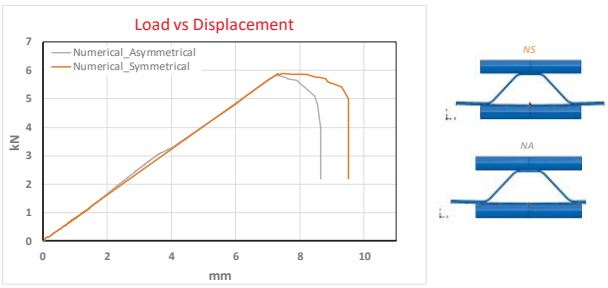

FIGURE 5. Comparison between Numerical_Symmetrical (NS) and Numerical_Asymmetrical (NA) models: load-displacement curves.

According to Figure 5, the NS and NA configurations has an equal peak load, while the maximum computed displacements are almost different. Once the peak load is reached, for both the configurations, intra-laminar and inter-laminar damages take place, leading to the collapse of the structure. Actually, damage propagation for symmetrical configuration is nearly gradual while a sudden drop in load carrying capability has been found for the *Numerical_Asymmetrical* configuration. The difference in the damage evolution between the two aforementioned models is related to their different geometry. Indeed, due to the wider area of the stringer foot, in the *Numerical_Symmetrical* configuration, a more uniform distribution of the stresses is allowed, at both the edges of the panel, with respect to the *Numerical_Asymmetrical* configuration.

The effect of the orientation of the roll on the load vs. imposed displacement curves is introduced in Figure 6, where the results of the *Numerical_Asymmetrical* and *Numerical_Asymmetrical_RollerRotation* models are compared.

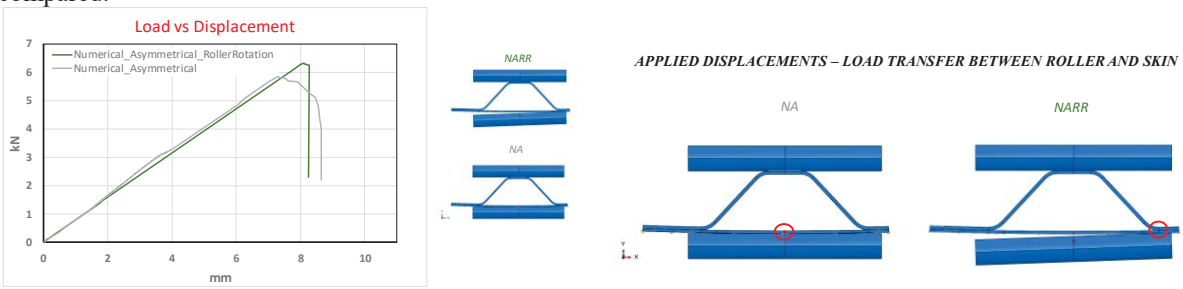

(a) (b)

FIGURE 6. Comparison between Numerical_Asymmetrical (NA) and Numerical_Asymmetrical_RollerRotation (NARR) models: (a) load-displacement curves; (b) contact point between roller and skin.

In Figure 6-a, the *Numerical_Asymmetrical_RollerRotation* configuration shows a sudden damage propagation after the peak load, even more sudden than the one observed for the *Numerical_Asymmetrical* configuration. However, the peak load found for the configuration called *Numerical_Asymmetrical_RollerRotation* is 10% higher than the one found for the *Numerical_Asymmetrical* configuration. This difference in peak load, observed for the two configurations, can be attributed to the different points of application of the load. Indeed, in the *Numerical_Asymmetrical_RollerRotation* model, the load is transferred from the roller to the panel in a reinforced region at the stringer foot location, as highlighted by Figure 6-b.

The Symmetrical configuration and the configuration with the different orientation of the roller are compared in Figure 7 (taking into account the effects of geometrical and load application asymmetry). In Figure 7, as expected, the *Numerical_Asymmetrical_RollerRotation* configuration shows a higher peak load and a less gradual damage propagation if compared to the *Numerical_Symmetrical* configuration. Actually, the more homogeneous distribution of stresses and the more gradual damage evolution observed in the *Numerical_Symmetrical* configuration allows an increment in the achieved displacements of the 15.9% if compared to the *Numerical_Asymmetrical_RollerRotation* configuration.

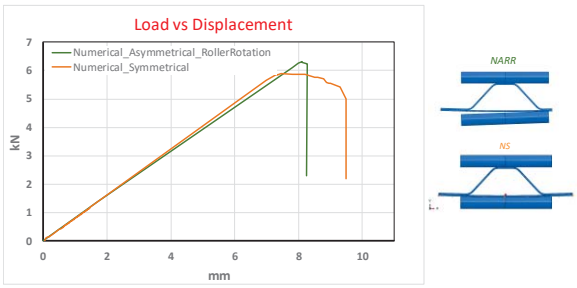

FIGURE 7. Comparison between Numerical_Symmetrical (NS) and Numerical_Asymmetrical_RollerRotation (NARR) models: load-displacement curves.

In order to assess the complete mechanical behavior induced by asymmetrical flexural conditions, in Figure 8, a comparison among the analyzed numerical configurations, in terms of intra-laminar and inter-laminar damages final status, is introduced. Figure 8 helps to justify the load displacements trends introduced in Figures 5, 6, and 7. Indeed, in terms of final inter-laminar damage status, significant differences can be observed for the three configurations. Obviously, a symmetrical evolution of the inter-laminar damage can be appreciated for the *Numerical_Symmetrical* configuration, while an asymmetrical distribution has been found for the *Numerical_Asymmetrical* configuration. Finally, a significantly larger delaminated area on the roller contact side can be appreciated for the *Numerical_Asymmetrical_RollerRotation* configuration.

The propagation of the intra-laminar damage for the analyzed configurations shows, as expected a wide and symmetrical damaged area for the *Numerical_Symmetrical* configuration; while a more marked asymmetrical distribution has been observed for the *Numerical_Asymmetrical* and *Numerical_Asymmetrical_RollerRotation* configurations. For the *Numerical_Asymmetrical_RollerRotation* configuration, the intra-laminar damaged area is significantly smaller and localized near the point of contact between the roller and the skin. This can explain the higher load peak and the sudden material degradation found for this last numerical configuration.

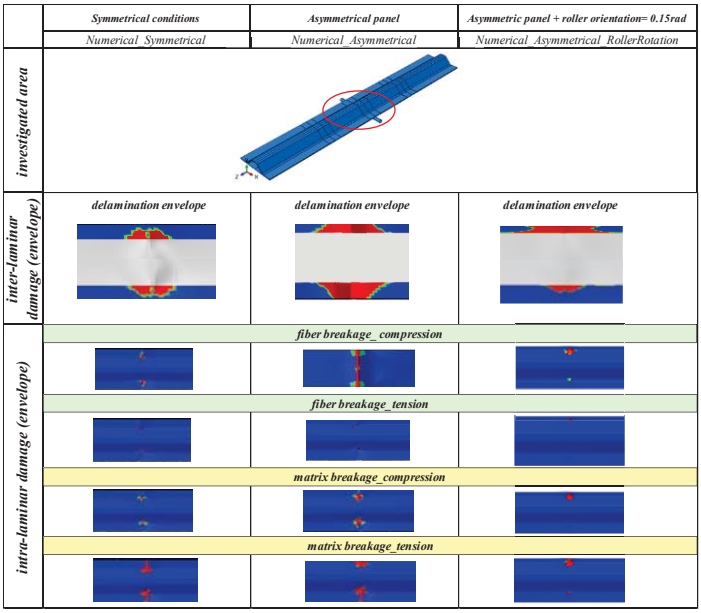

FIGURE 8. Comparison among the analyzed configurations: final damage status.

EXPERIMENTAL RESULTS AND VALIDATION OF THE NUMERICAL MODEL

The numerical model has been validated by comparing the obtained numerical outputs with experimental data from a three-point bending test on the *Numerical_Asymmetrical_RollerRotation* configuration. This configuration has been chosen to test the capability of the numerical model to take into account asymmetrical conditions related both to geometry and load application. The experimental test configuration is reported in Figure 9-a.

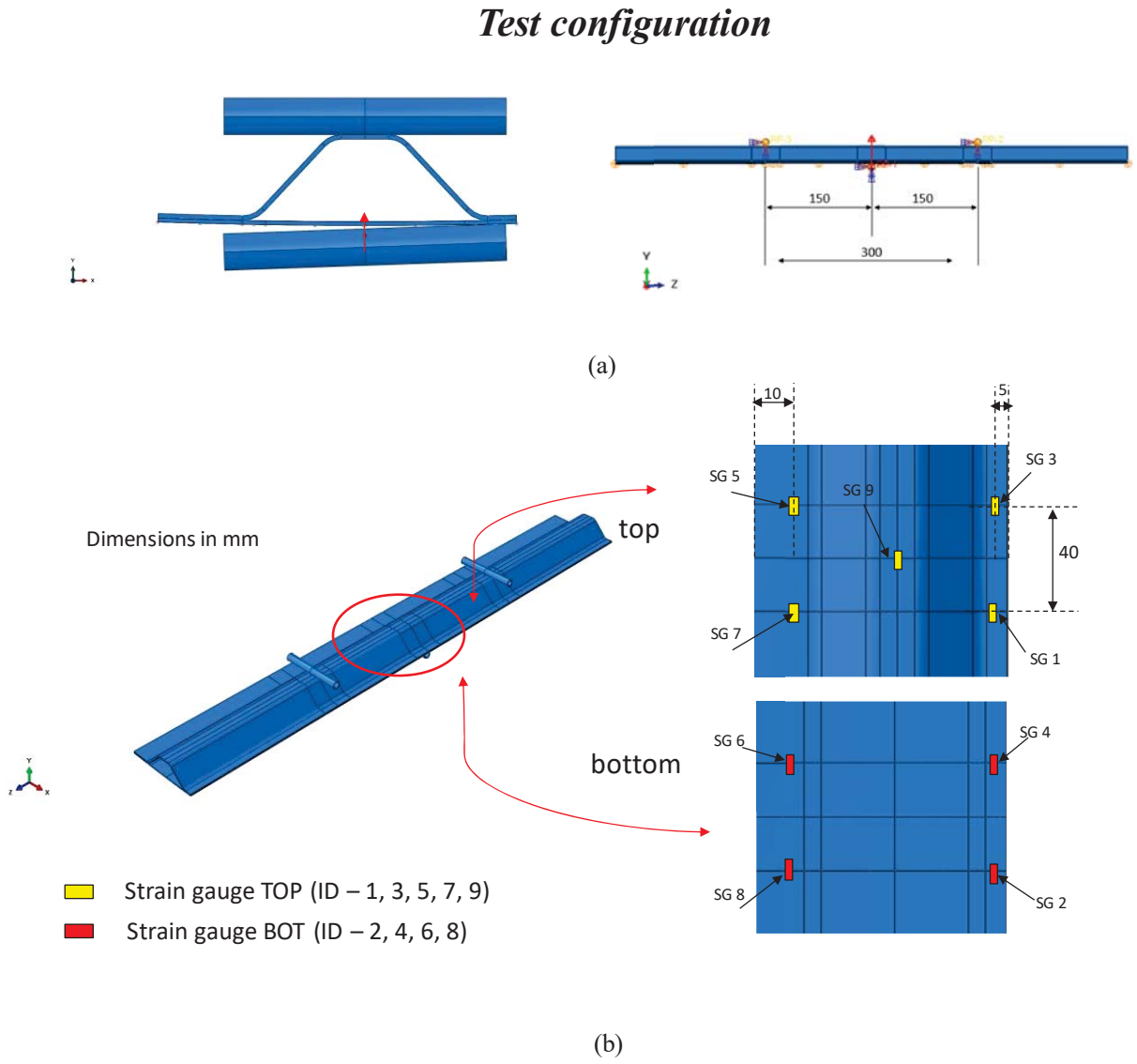

FIGURE 9. (a) Three points bending experimental test configuration; (b) Strain gauges position.

The experimental test has been performed at CIRA (*Centro Italiano di Ricerca Aerospaziale*), by means of the Instron 4505 test machine. Nine strain gauges have been used to monitor the local deformations on the composite panel during the test execution. The strain gauges position is reported in Figure 9-b, both for top and bottom surfaces. The test rig is shown in Figure 10. A 10 mm displacement has been applied at a rate of 1 mm/min. At 8.28 mm applied displacement the panel failed under flexural load. The damage is clearly visible in Figure 11.

(a) (b)

FIGURE 10. Test rig: (a) isometric view, (b) front view.

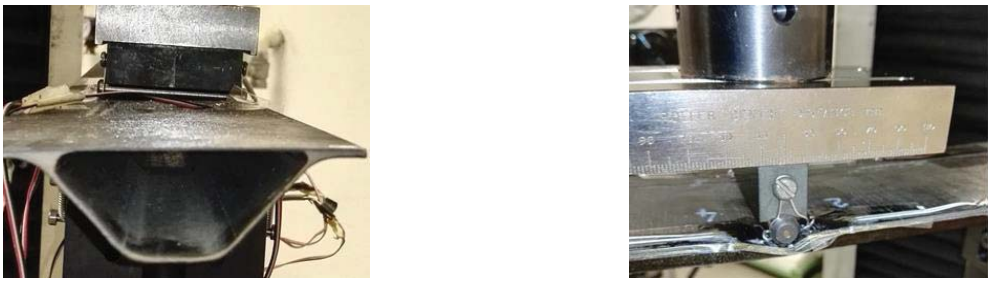

(a) (b)

FIGURE 11. Failure (a) front view, (b) detail.

2In Figure 12-a, the numerical and the experimental data are compared in terms of load-displacement curves, while strain gauge 09 reading as a function of the reaction force is introduced in Figure 12-b. From this figure, the numerical model is able to mimic the global stiffness of the panel and in general the global flexural behavior, by providing reasonable predictions in terms of peak load, maximum displacements, damage propagation rate and strain distribution.

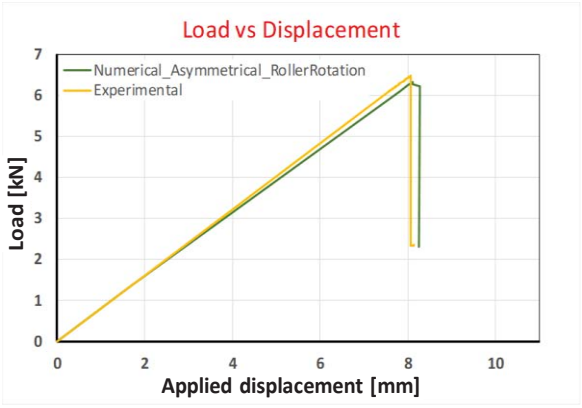

(a)

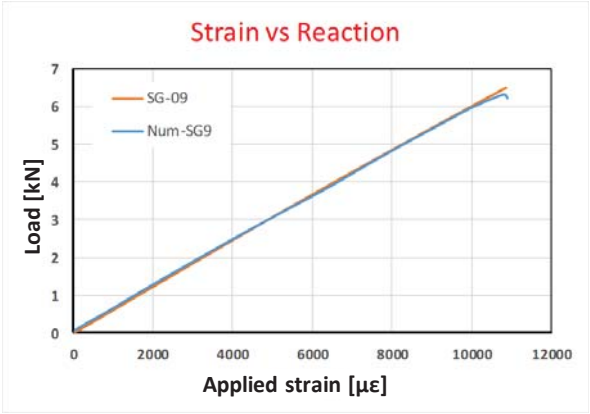

(b)

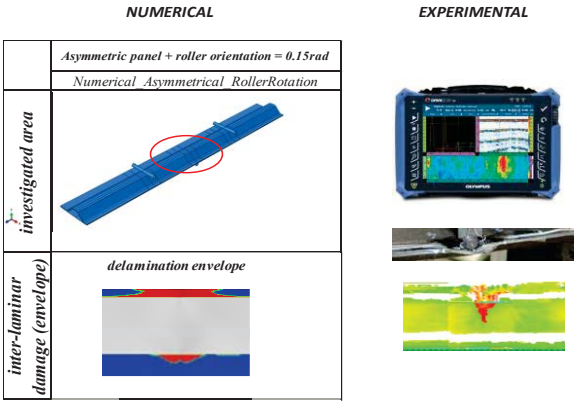

(c)

FIGURE 12. (a) experimental and numerical load-displacement curves comparison; (b) experimental and numerical strain-reaction comparisons; (c) Numerically predicted Inter-laminar final damage status Vs NDI inspections

In Figure 12-c, the numerically predicted inter-laminar damage final status and the images of non-destructive inspections performed with the *Omniscan-Olympus* ultrasonic phased array instrument are compared. From this figure, a limitation of the numerical model can be pointed out, which does not affect the prediction of the global flexural behavior, but strongly influence the prediction of the inter-laminar damage evolution locally. Indeed, in the frame of the numerical test, inter-laminar damages are not able to propagate along the thickness among the skin plies, because, in order to reduce the computational cost, cohesive elements have been placed only at skin stringer interface. On the other hand, the propagation of inter-laminar damages along the thickness can be clearly appreciated from the ultrasonic non-destructive test images (see Figure 12-c). Therefore, as can be appreciated in Figure 12-c, in the frame of the numerical analyses, delamination propagates along the panel axial direction. As already remarked, this discrepancy does not influence the effectiveness of the global prediction supplied by the model which has been found able to provide useful complementary information (with respect to experimental data) on the influence of boundary conditions on the asymmetrical flexural behavior of the investigated panel.

CONCLUSIONS

This work presents a numerical/experimental investigation on the asymmetrical bending behavior of a composite panel reinforced with omega composite stringer. A three-point bending test has been performed on an asymmetrical configuration selected by means of a preliminary numerical study performed with the aid of a numerical model capable to predict intra-laminar and inter-laminar damage onset and evolution.

The preliminary numerical investigation on the influence of asymmetry in geometry and in loading conditions on the whole flexural behavior of the panel has revealed that the asymmetrical configuration develops a less distributed inter-laminar and intra-laminar damage which leads to a sudden degradation and drop of load. These conclusions have been confirmed by the three-point experimental bending test, whose experimental outputs in terms of global stiffness, load-displacement curve, strain distributions, and damage propagation measured by means of non-destructive ultrasonic inspections, have been found in excellent agreement with the numerical predictions. Limitations in the capability of the introduced Finite Elements numerical model to predict the intra-laminar final damage status at local level have been pointed out, which have found to not affect its capability to predict the whole flexural behavior of the investigated stiffened panel.

REFERENCES

1. T. Sadowski and P. Golewski, Archives of Metallurgy and Materials **60**(4), 2813–2820 (2015).
2. Ch. Affolter, G. Piskoty, L. Wullschleger, and B. Weisse, Engineering Failure Analysis **16**(6), 1846–1855 (2009).
3. R. Studzinski, Z. Pozorski, and A. Garstecki, Journal of Constructional Steel Research **104**, 227–234 (2015).
4. J.M. Lawrence, AIAA Journal **11**(6), 793–800 (1973).
5. K. Chandrashekhara and B.S. Kumar, Acta Mechanica **84**(1–4), 63–75 (1990).
6. K. Chandrashekhara and B.S. Kumar, Composite Structures **23**(1), 1–9 (1993).
7. M.K. Cvitkovich, R. Krueger, T.K. O'Brien, and P.J. Minguet, "Debonding in composite skin/stringer configurations under multi-axial loading" in *Proceedings of the 13th Annual Technical Conference on Composite Materials*, 1998.
8. M. Akterskaia, E. Jansen, S.R. Hallett, P. Weaver, and R. Rolfes, Composite Structures **202**, 1280–1294 (2018).
9. R. Krueger, M.K. Cvitkovich, T.K. O'Brien, and P.J. Minguet, Journal of composite Materials **34**(15), 1263–1300 (2000).
10. P.J. Minguet and T.K. O'Brien, in: *Composite Materials, Testing and Design: Twelfth Volume*. ASTM International, 1996.
11. J. Bertolini, B. Castanié, J.-J. Barrau, and J.-P. Navarro, Composite Structures **86**(1–3), 233–242 (2008).
12. C.G. Daville, P.P. Camanho, M.F. deMoura, Progressive damage analyses of skin/stringer debonding, NASA Technical Report, 2004.
13. A. Riccio, R. Cristiano, S. Saputo, A. Sellitto, Composite Structures **202**, 590–602 (2018).
14. F. Di Caprio, D. Cristillo, S. Saputo, M. Guida, A. Riccio, Composite Structures **216**, 39–52 (2019).
15. A. Riccio, A. Raimondo, S. Saputo, A. Sellitto, M. Battaglia, G. Petrone, Composite Structures **202**, 909–916 (2018).